Published in final edited form as:
J Mech Behav Biomed Mater. 2012 November ; 15: 208–217. doi:10.1016/j.jmbbm.2012.07.001.

Evidence of Adaptive Mitral Leaflet Growth

Manuel K. Rausch[a,b], **Frederick A. Tibayan**[c], **D. Craig Miller**[d], and **Ellen Kuhl**[a,b,d,e,*]

[a]Department of Mechanical Engineering, Stanford, California, USA [b]Department of Mechanical and Process Engineering, ETH Zurich, Zurich, Switzerland [c]Department of Surgery, Oregon Health and Science University, Portland, Oregon, USA [d]Department of Cardiothoracic Surgery, Stanford, California, USA [e]Department of Bioengineering, Stanford, California, USA

Abstract

Ischemic mitral regurgitation is mitral insuffciency caused by myocardial infarction. Recent studies suggest that mitral leaflets have the potential to grow and reduce the degree of regurgitation. Leaflet growth has been associated with papillary muscle displacement, but role of annular dilation in leaflet growth is unclear. We tested the hypothesis that chronic leaflet stretch, induced by papillary muscle tethering and annular dilation, triggers chronic leaflet growth. To decipher the mechanisms that drive the growth process, we further quantified regional and directional variations of growth. Five adult sheep underwent coronary snare and marker placement on the left ventricle, papillary muscles, mitral annulus, and mitral leaflet. After eight days, we tightened the snares to create inferior myocardial infarction. We recorded marker coordinates at baseline, acutely (immediately post infarction), and chronically (five weeks post infarction). From these coordinates, we calculated acute and chronic changes in ventricular, papillary muscle, and annular geometry along with acute and chronic leaflet strains. Chronic left ventricular dilation of 17.15% ($p<0.001$) induced chronic posterior papillary muscle displacement of 13.49mm ($p=0.07$). Chronic mitral annular area, commissural and septal-lateral distances increased by 32.50% ($p=0.010$), 14.11% ($p=0.007$), and 10.84% ($p=0.010$). Chronic area, circumferential, and radial growth were 15.57%, 5.91%, and 3.58%, with non-significant regional variations ($p=0.868$). Our study demonstrates that mechanical stretch, induced by annular dilation and papillary muscle tethering, triggers mitral leaflet growth. Understanding the mechanisms of leaflet adaptation may open new avenues to pharmacologically or surgically manipulate mechanotransduction pathways to augment mitral leaflet area and reduce the degree of regurgitation.

Keywords

growth; remodeling; cardiac mechanics; mitral valve; mitral leaflet; regurgitation

1. INTRODUCTION

Mitral regurgitation, the inability of the mitral valve to close properly, is associated with increased morbidity and mortality [30]. Functional mitral regurgitation, as seen in patients with ischemic or idiopathic dilated cardiomyopathy, is a result of annular and subvalvular

*corresponding author, phone: +1.650.450.0855, fax: +1.650.725.1587, ekuhl@stanford.edu, url: http://biomechanics.stanford.edu.

alterations secondary to left ventricular remodeling [14, 18]. A recent study has shown that mitral leaflets of patients with ischemic or idiopathic dilated cardiomyopathy are significantly larger than leaflets of normal patients [3]. The same study demonstrated that patients with enlarged leaflets display a smaller degree of regurgitation than patients with normal leaflets. These findings motivate the hypothesis that adaptive mitral leaflet growth might be a compensatory mechanism for left ventricular remodeling.

In a controlled ovine model of tachycardia-induced dilated cardiomyopathy, mitral leaflets elongated chronically in the radial direction [27]. In an ovine model with inferior myocardial infarction, the entire leaflet area increased in response to left ventricular remodeling [4]. In an ovine model of isolated apical papillary muscle displacement, not only leaflet area but also leaflet thickness increased chronically in response to elevated mechanical stresses induced by papillary muscle tethering [5]. The same study reported significant changes in cell phenotype, secondary to the reactivation of embryonic gene profiles. Taking advantage of mechanotransduction is a powerful approach to endogenously engineer new tissue [13, 31]. This concept has been applied successfully to induce controlled in situ growth of thin biological membranes in plastic and reconstructive surgery [2, 6]. The potential to manipulate leaflet area by stretch would open exciting new avenues for a pharmacologically or surgically targeted reduction of the degree of mitral regurgitation.

While recent technologies enable the precise characterization of leaflet area in vivo using three-dimensional echocardiography [5], these methods are not suited to quantify chronic regional and directional leaflet growth on a local level. Since leaflet valves display strong regional and directional variations [20, 25], this regional and directional information could provide valuable insight into the mechanistic origin of leaflet growth. Here, rather than using global information from standard imaging technologies, we follow discrete anatomic landmarks over an extended period of time [1, 15]. This allows us to precisely quantify regional and directional growth across the entire anterior mitral leaflet [8]. Using a chronic infarct ovine model, we test the hypothesis that chronic leaflet stretch, induced by papillary muscle tethering and annular dilation, triggers a chronic increase in leaflet area. We further hypothesize that this leaflet area growth is a result of both circumferential and radial leaflet elongation.

2. MATERIALS AND METHODS

All animals received humane care in compliance with the Principles of Laboratory Animals Care formulated by the National Academy of Sciences and published by the National Institute of Health. This study was approved by the Stanford Medical Laboratory Research Animals Review Committee and conducted according to Stanford University policy.

2.1. Surgical Preparation

We premedicated five Dorsett hybrid sheep (71 ± 5kg) with ketamine (25mg/kg intramuscularly), anesthetized them intravenously with sodium thiopental (6.8mg/kg IV), and maintained anesthesia with inhalational isoflurane (1% to 2.5%). Through a left thoracotomy, we established access to the heart. We placed eight markers onto the epicardial surface of the left ventricle along four equally spaced longitudinal meridians and added a ninth marker at the apex. To induce controlled myocardial infarction, we placed polypropylene 2-0 sutures around the second and third obtuse marginal branches of the left circumflex coronary artery and snared them loosely [16].

On cardiopulmonary bypass with the heart arrested, we sewed additional markers onto the tips of both papillary muscles, two markers each, to the anterior, lateral, and posterior portions of the endocardium in the equatorial plane. Last, we sewed a total of 17 markers to

the mitral valve, eight to the annulus, five to the anterior leaflet, and four to the posterior leaflet, see Figures 1 and 2. To measure the left ventricular pressure, we used a micromanometer pressure transducer (PA4.5-X6, Konigsberg Instruments Inc., Pasadena, CA). Once the animals were weaned off cardiopulmonary bypass, we externalized the tourniquets for the coronary artery snares through the fifth intercostal space and buried them in a subcutaneous pocket.

2.2. Experimental Protocol

After 8 ± 2 days, we took the animals to the cardiac catheterization laboratory, where we sedated them intravenously with ketamine (1 to 4 mg/kg/h) and diazepam (5mg), and maintained sedation with inhalational isoflurane (1% to 2.5%). With the animal in the right decubitus position, we acquired baseline marker coordinates via biplane videofluoroscopy at a sampling frequency of 60 Hz (Philips Medical Systems, Pleasanton, CA). Simultaneously, we recorded aortic pressure, left ventricular pressure, and ECG signals. Following medication with lidocaine (100 mg IV), bretylium (75 mg IV), and magnesium (3 g IV), we tightened the coronary snares and verified complete vessel occlusion angiographically. Immediately post-infarction, we acquired acute condition marker coordinates via biplane videofluoroscopy along with the left ventricular pressure. After 5 ± 1 weeks, the animals returned to the cardiac catheterization laboratory to record chronic condition marker coordinates via biplane videofluoroscopy along with hemodynamic measurements. After the animals were sacrificed, we verified proper marker attachment. Off-line, we extracted four-dimensional marker coordinates from the biplane videofluoroscopic images [17, 26].

2.3. Data Analysis

For the analysis, we distinguished three conditions: baseline, prior to myocardial infarction; acute, immediately post-infarction; and chronic, 5 ± 1 weeks post-infarction.

2.3.1. Hemodynamics—From the recorded left ventricular pressure curves, we determined characteristic time points of the cardiac cycle. We defined End Diastole (ED) as the time point immediately prior to left ventricular pressure upstroke and End Systole (ES) as the time point of peak negative rate of left ventricular pressure drop. We calculated Left Ventricular End Diastolic Volume (LVEDV) and Left Ventricular End Systolic Volume (LVESV) by approximating the left ventricle as a prolate ellipsoid using the left ventricular and annular markers.

2.3.2. Cardiac Remodeling—To elucidate potential mechanisms that trigger mitral leaflet growth, we quantified acute and chronic changes in cardiac geometry in response to myocardial infarction. We calculated annular, ventricular, and papillary muscle changes, both between baseline and acute conditions (acute) and between baseline and chronic conditions (chronic). To characterize annular changes, we followed a method previously described [22, 24], and calculated percentage changes in Septal-Lateral distance (SL, distance between markers 1 and 5), Commissure-Commissure distance (CC, distance between markers 3 and 7), Mitral Annular Area (MAA, area enclosed by the marker polygon 1–8), Saddle Height (SH, average distance between marker 1 and markers 3 and 7 projected onto the normal of the best fit plane through all annular markers), Anterior Perimeter (AP, sum of the distances between markers 8-2), and Posterior Perimeter (PP, sum of the distances between markers 2–8), see Figure 2A. To characterize ventricular changes, we calculated changes in left ventricular volume, enclosing both the left ventricular cavity and the myocardium. To characterize papillary muscle changes, we calculated apical, lateral, and posterior components of the vectors pointing from the saddlehorn marker 1, to the posterior and anterior papillary muscles. We defined the apical direction along the long axis of the left ventricle, i.e., the direction pointing from the geometric center of the annular

markers 1–8 to the apex marker. We defined the posterior and lateral directions using markers 3 and 7 and using markers 1 and 5, respectively, see Figure 2A.

2.3.3. Mitral Leaflet Growth—To characterize mitral leaflet growth, we quantified acute and chronic mitral leaflet strains in response to myocardial infarction. We calculated area, circumferential, and radial strains, both between baseline and acute conditions (acute strains) and between baseline and chronic conditions (chronic strains). Since sensitivity studies have demonstrated that strain profiles are relatively insensitive to the choice of reference configuration [21], we selected minimal Left Ventricular Pressure (LVP-min) as time point of comparison to minimize effects of possible additional elastic strains, see Figure 3. From five markers on the leaflet and three markers on the septal region of the annulus, we created a mesh consisting of eight nodes and eight triangular elements, see Figure 2. We characterized the leaflet as a thin membrane [19], and quantified its strain state exclusively in terms of its membrane strains [1, 21]. For each three-noded membrane element, $n_{\text{nod}} = 3$, we interpolated the reference configuration under baseline conditions $\boldsymbol{X}(\theta^1,\theta^2)$ and the current configuration under acute and chronic conditions $\boldsymbol{x}(\theta^1,\theta^2)$ in terms of the reference and current marker coordinates $\boldsymbol{X}_I$ and $\boldsymbol{x}_I$ [29].

$$\begin{aligned}\boldsymbol{X}(\theta^1,\theta^2)&=\textstyle\sum_{I=1}^{n_{\text{nod}}} N_I(\theta^1,\theta^2)\boldsymbol{X}_I\\ \boldsymbol{x}(\theta^1,\theta^2)&=\textstyle\sum_{I=1}^{n_{\text{nod}}} N_I(\theta^1,\theta^2)\boldsymbol{x}_I\end{aligned} \quad (1)$$

Here, N_I are the linear shape functions parameterized in terms of the local curvilinear coordinates θ^α with $\alpha = 1, 2$. From their partial derivatives with respect to the curvilinear coordinates $\partial N_I/\partial\theta^\alpha$, we calculated the sets of covariant base vectors in the reference configuration $\boldsymbol{G}_\alpha$ and in the current configuration $\boldsymbol{g}_\alpha$.

$$\begin{aligned}\boldsymbol{G}_\alpha(\theta^1,\theta^2)&=\textstyle\sum_{I=1}^{n_{\text{nod}}}\frac{\partial N_I}{\partial\theta^\alpha}\boldsymbol{X}_I\\ \boldsymbol{g}_\alpha(\theta^1,\theta^2)&=\textstyle\sum_{I=1}^{n_{\text{nod}}}\frac{\partial N_I}{\partial\theta^\alpha}\boldsymbol{x}_I\end{aligned} \quad (2)$$

From the scalar product between the individual covariant base vectors, we calculated the covariant surface metrics of the reference configuration $G_{\alpha\beta}$ and of the current configuration $g_{\alpha\beta}$.

$$G_{\alpha\beta}=\boldsymbol{G}_\alpha\cdot\boldsymbol{G}_\beta \quad g_{\alpha\beta}=\boldsymbol{g}_\alpha\cdot\boldsymbol{g}_\beta \quad (3)$$

Using the contravariant spatial surface metric $g^{\alpha\beta} = [g_{\alpha\beta}]^{-1}$, i.e., the inverse of the covariant spatial surface metric $g_{\alpha\beta}$, we mapped the covariant base vectors $\boldsymbol{g}_\beta$ onto their contravariant counterparts $\boldsymbol{g}^\alpha$.

$$\boldsymbol{g}^\alpha=g^{\alpha\beta}\boldsymbol{g}_\beta \quad g^{\alpha\beta}=\boldsymbol{g}^\alpha\cdot\boldsymbol{g}^\beta=[g_{\alpha\beta}]^{-1} \quad (4)$$

We then calculated the Euler-Almansi membrane strains $\boldsymbol{e}$ as the differences between the contravariant current and reference surface metrics $g_{\alpha\beta}$ and $G_{\alpha\beta}$ in terms of the contravariant spatial base vectors $\boldsymbol{g}^\alpha$.

$$\boldsymbol{e}=e_{\alpha\beta}\,\boldsymbol{g}^\alpha\otimes\boldsymbol{g}^\beta \quad e_{\alpha\beta}=\frac{1}{2}[g_{\alpha\beta}-G_{\alpha\beta}] \quad (5)$$

To determine the circumferential strains e^{circ} and stretches λ^{circ}, we mapped the Euler-Almansi strain $\boldsymbol{e}$ onto the circumferential directions $\boldsymbol{n}^{\text{circ}}$ generated as the unit vector between markers 2 and 8 in the current configuration, see Figure 2A.

$$e^{\text{circ}} = \boldsymbol{n}^{\text{circ}} \cdot \boldsymbol{e} \cdot \boldsymbol{n}^{\text{circ}} \qquad \lambda^{\text{circ}} = [\,1 - 2e^{\text{circ}}\,]^{-1/2} \quad (6)$$

To determine the radial strains e^{rad} and stretches λ^{rad}, we mapped the Euler-Almansi strain $\boldsymbol{e}$ onto the radial direction $\boldsymbol{n}^{\text{rad}}$ generated as the unit vector between markers 1 and 9 in the current configuration, see Figure 2A.

$$e^{\text{rad}} = \boldsymbol{n}^{\text{rad}} \cdot \boldsymbol{e} \cdot \boldsymbol{n}^{\text{rad}} \qquad \lambda^{\text{rad}} = [\,1 - 2\,e^{\text{rad}}\,]^{-1/2} \quad (7)$$

Finally, we calculated the Euler-Almansi area strains e^{area} and stretches λ^{area} as the relative changes in triangular area, where dA and da are the areas of each triangular element in the reference and current configurations.

$$e^{\text{area}} = \frac{\text{da} - \text{dA}}{\text{da}} \qquad \lambda^{\text{area}} = \frac{\text{da}}{\text{dA}} = \frac{1}{[\,1 - e^{\text{area}}\,]} \quad (8)$$

We averaged all strains and stretches for three consecutive cardiac cycles, see Figure 3. In the following, we interpret the resulting circumferential strains e^{circ}, radial strains e^{rad}, and area strains e^{area} as measures for acute and chronic growth [9, 23]. In Figure 4, we report means and standard deviations of acute and chronic area, circumferential, and radial strains, grouped into five regions, Free Edge (FE), Central Belly (CB), Anterior Annulus (AA), Posterior Commissure (PC), and Anterior Commissure (AC), see Figure 2B. In Figure 5, we report chronic area, circumferential, and radial strains for all five animals on a smoothed and refined leaflet geometry using the method of subdivision surfaces [8]. Systematic sensitivity studies have demonstrated that subdivision surface techniques can be used for smoothing and refinement of leaflet geometries without affecting the underlying strain profiles [21].

2.4. Statistical Analysis

We report all data as mean ± 1 standard deviation. In Table 1, we compared hemodynamic data for baseline, acute, and chronic conditions using repeated-measure-Anova. In the case were the sphericity assumption was violated according to Mauchlys test, we applied the Greenhouse-Geisser correction. In Table 2 and in Figure 4, we tested changes in annular and ventricular geometry and strain components in all five regions, respectively, for being larger than zero, both acutely and chronically, using one-sided student t-tests. In Table 2, we compared papillary muscle displacements to zero using two-sided student t-tests. To test whether these metrics were larger chronically than acutely, we applied one-sided paired student t-tests. In Figure 4, we compared strains between different regions using One-Way Anova or Welch test, where the equal variance assumption was violated according to Levenes test. We performed multi-comparison using Bonferroni Post-hoc test unless equal variance assumption was violated for One-Way Anova, in which case we performed Games-Howell Post-hoc test. For all statistical tests, we defined the level of statistical significance as 0.05.

3. RESULTS

We successfully acquired hemodynamic data and four-dimensional marker coordinates for all five sheep under baseline conditions, acutely immediately post-infarction, and chronically 5 ± 1 weeks post-infarction.

3.1. Hemodynamics

Table 1 summarizes baseline, acute, and chronic hemodynamics. We found statistically significant differences between conditions for heart rate (p=0.027) and dP/dt (p=0.012) using repeated-measure-Anova. Heart rate under chronic conditions was significantly smaller than under normal conditions (p=0.026). Multi-comparison did not show differences between the means of the groups for dP/dt.

3.2. Cardiac Remodeling

Table 2 summarizes acute and chronic changes in cardiac geometry. Under acute conditions, changes in annular geometry were negligible. Only SH showed a significant decrease (−39.61% ± 16.02, p=0.003), whereas acute alterations in all other metrics remained statistically non-significant. Under chronic conditions, we observed noteworthy annular remodeling. At end-diastole, changes in SL (10.84% ±6.48, p=0.010), CC (14.11% ± 7.48, p=0.007), MAA (32.50% ± 19.66, p=0.010), AP (15.32% ± 5.15, p=0.003), and PP (14.22% ± 7.04, p=0.007) were significantly larger than zero. At end-systole, changes in CC (9.52% ± 5.53, p=0.009), MAA (18.34% ± 12.17, p=0.014), AP (6.93% ± 5.85, p=0.008), and PP (9.93% ± 7.06, p=0.011) were all significantly larger than zero. Chronic changes were significantly larger than acute changes at end-diastole for SL (p=0.006), CC ($p<0.001$), MAA (p=0.002), AP (p=0.007), PP (p=0.001) and at end-systole for CC (p=0.002), MAA (p=0.020), AP (p=0.008), and PP (p=0.014). Under acute conditions, there was no significant increase in ventricular volume. Under chronic conditions, ventricular volume increased significantly at end-diastole (17.15% ± 4.56, $p<0.001$) and at end-systole (15.48% ± 5.81, p=0.002). Ventricular changes were significantly larger under chronic conditions than under acute conditions, both at end-diastole (p=0.002) and end-systole (p=0.001).

Both papillary muscles were displaced under acute conditions at end-systole. Under acute conditions, the posterior papillary muscle displaced in lateral direction (2.82mm ± 1.71, p=0.021) and the anterior papillary muscle displaced in apical direction (0.82mm ± 0.41, p=0.011), in lateral direction (1.07mm ± 0.68, p=0.024), and in anterior direction (1.48mm ± 0.91, p=0.022). Under chronic conditions, the posterior papillary muscle displaced in lateral direction at end-systole (4.21mm ± 3.76, p=0.067) and in posterior direction at both, end-diastole (13.49mm ± 12.31, p=0.070) and end-systole (11.89mm ± 11.30, p=0.078), however we could not show statistical significance. Under chronic conditions, the anterior papillary muscle displaced in apical direction at end-diastole (-3.29 ± 1.37, p=0.006). Chronic posterior papillary muscle displacements were significantly larger than acute posterior papillary muscle displacements in posterior direction, both at end-diastole (p=0.012) and end-systole (p=0.016). Chronic anterior papillary muscle displacements were significantly larger than acute displacements only in apical direction at end-diastole (p=0.013).

3.3. Mitral Leaflet Growth

Figure 4 summarizes the area, circumferential, and radial strains in all five regions, free edge, central belly, anterior annulus, posterior commissure, and anterior commissure.

Under acute conditions, area strains were not significantly larger than zero in any region. Under chronic conditions, area strains were significantly larger than zero in the central belly

(20.92% ± 13.91, $p < 0.001$), anterial annulus (13.25% ± 12.23, p=0.004), and anterior commissure (13.50% ±10.15, p=0.031) regions. We found no significance in the free edge (14.35% ± 25.69, p=0.056) and posterior commissure (15.11% ± 20.00, p=0.087) regions. Chronic area strain of all five regions on average was 15.57%. For all five regions, area strains were significantly larger chronically than acutely (free edge: p=0.038, central belly: $p < 0.001$, anterior annulus: p=0.001, posterior commissure: p=0.043, anterior commissure: p=0.020). One-way Anova revealed no difference between the five regions (p=0.868).

Under acute conditions, circumferential strains were not larger than zero in any region. Under chronic conditions, circumferential strains were larger than zero in the central belly (7.15% ± 4.36, $p < 0.001$), anterior annulus (8.21% ± 5.83, $p < 0.001$), and anterior commissure (4.52% ± 2.18, p=0.005) regions. We found no significance in the free edge (3.06% ±8.23, p=0.135) and posterior commissure (5.83% ± 5.90, p=0.061) regions. Chronic circumferential strain of all regions on average was 5.91%. For all five regions, circumferential strains were significantly larger chronically than acutely (free edge: p=0.046, central belly: $p < 0.001$, anterior annulus: $p < 0.001$, posterior commissure: p=0.040, anterior commissure: $p < 0.001$). One-way Anova revealed no difference between the five regions (p=0.382).

Under acute conditions, radial strains were not significantly larger than zero in any region. Under chronic conditions, radial strains were larger than zero only in the central belly region (10.89% ± 10.51, p=0.005). We found no significance in the free edge (−4.66% ± 12.80, p=0.860), anterior annulus (3.73% ± 9.02, p=0.112), posterior commissure (3.31% ± 9.10, p=0.225), and anterior commissure (5.27% ± 10.74, p=0.167) regions. Chronic radial strain of all regions on average was 3.58%. In the central belly (p=0.003), anterior annulus (p=0.012), and posterior commissure (p=0.040) regions, radial strains were significantly larger chronically than acutely. One-Way Anova revealed significant difference between groups (p=0.047). Bonferroni post-hoc showed a significant difference between the free edge and central belly regions (p=0.025). Figure 5 shows the kinematic reconstruction of the anterior mitral leaflet for all five animals under both baseline and chronic conditions. To enhance orientation, we have overlaid a smooth representation of the mitral valve annulus, fit through the annular marker points [22, 24]. The color code corresponds to the chronic leaflet strain between baseline and chronic conditions at minimum left ventricular pressure, which we interpret as a growth [10, 23]. Figure 5, first row, displays the five anterior mitral leaflets under baseline conditions. Figure 5, second row, illustrates the inter-subject variation in chronic area strains, with animals 2 and 5 showing largest area growth, while animal 1 showed almost no growth. Chronic area strains displayed significant regional variations and were heterogeneous across the leaflets. Figure 5, third row, displays the chronic circumferential strains. Circumferential growth seems to be largest in the posterior region of the leaflet. However, these changes were statistically non-significant, as confirmed in Figure 4. Figure 5, fourth row, shows the chronic radial strains, which behave qualitatively similarly to the chronic area strains. Again, animals 2 and 5 showed largest radial growth, while animal 1 showed almost no growth.

4. DISCUSSION

4.1. Summary

We have presented a regional and directional quantification of mitral leaflet growth under acute and chronic ischemic conditions. Using a four-dimensional imaging technology that has been widely used in our laboratory, we were able to show significant remodeling of the ovine heart following an ischemic event. We have demonstrated that the anterior mitral leaflet increases its area chronically compared to both baseline and acute post-infarct conditions. Leaflet area growth was homogeneous on average, with only minor regional

variations. Leaflet growth was anisotropic, with slightly larger growth in the circumferential than in the radial direction.

4.2. Growth Stimuli

To induce controlled leaflet growth, it is critical to understand the driving biochemical and mechanical stimuli that trigger a compensatory area increase [7]. There is general agreement that leaflet stretch beyond a physiological limit may act as a mechanical stimulus for growth [3, 4, 5]. One way to stretch the mitral valve leaflet is a controlled apical displacement of the papillary muscles, which has been shown to induce leaflet growth, even in the absence of ischemic events [5]. However, because the mitral annuli remodeled as well in this study, it remained unclear to which extent leaflet growth could be attributed to papillary muscle tethering alone. Other studies have demonstrated that the leaflet area-to-annular area ratio remains constant, even under significant infarct-induced annular dilation [12]. In contrast to all previous echocardiography-based studies, our marker-based study allows us to precisely follow discrete anatomic landmarks in time and space [28, 29]. Four-dimensional marker coordinates provide access to acute and chronic, regional and directional strain profiles across the entire mitral leaflet [1, 21]. Qualitatively, our chronic strain contour plots in Figure 5 suggest regional variations of leaflet growth. Quantitatively, however, we were not able to show statistically significant differences in chronic area, circumferential, and radial strains between the different leaflet regions in Table 2. The lack of statistically significant regional and directional variation in leaflet growth might be attributed to the small number of study subjects, n=5. Alternatively, lack of regional variation might suggest mechanotransduction pathways triggered by global stimuli such as stretch, which could initiate a global rather than a local membrane growth [6, 31].

4.3. Comparison with Previous Studies

A decade ago, an ex vivo study of mitral leaflets of patients with dilated cardiomyopathy revealed larger leaflet areas than those of patients without a known history of cardiac disease [12]. In this cadaveric study, the authors found a total increase of leaflet area of approximately 24% in hearts with ischemic dilated cardiomyopathy and an increase of approximately 50% in hearts with idiopathic dilated cardiomyopathy in comparison to hearts without known pathologic conditions. These findings motivated the hypothesis that leaflet growth is a compensatory mechanism in response to mitral valve insuffciency.

Subsequently, several groups began to study mitral leaflet remodeling in humans in vivo using echocardiography [3, 11]. In the first study, anterior and posterior mitral leaflets were 28% and 41% longer in patients with congestive heart failure when compared to normal patients [11]. In the second study, leaflet area was 33% to 38% larger leaflets of patients with left ventricular abnormalities when compared to normal patients [3]. Our group was the first to provide evidence of remodeling in a pre-post study under controlled conditions, in which sheep with tachycardia-induced dilated cardiomyopathy displayed leaflet lengthening of 23% in the anterior leaflet and 24% in the posterior leaflet [27]. Our findings were confirmed by two follow up studies, which reported an increase in leaflet area similar to previous findings, with 38% area increase in ischemic dilated cardiomyopathy and 17% area increase in response to leaflet stretching following isolated papillary muscle displacement [4, 5].

In comparison to these previous studies, the area growth of 16% observed in our study is slightly smaller. This may be attributed to the short duration of our study. With 5 ±1 weeks, our growth and remodeling period is much shorter than the other reported studies, which were several months long [4, 5]. Our observation that growth takes place in both

circumferential and radial directions, with slightly larger circumferential growth, agrees qualitatively with reported observations [7].

4.4. Limitations

First, this study used a chronic ovine model with interior infarction, which is inherently different from human infarct patients [3]. Second, prior to infarction, all sheep had undergone opening of the pericardium and the heart, cardiopulmonary bypass, and surgical manipulation for marker placement. This implies that the surgical procedure itself cannot be excluded as a cause for the remodeling phenomena observed in the present study. Third, the duration of the study was relatively short in comparison to the original eight-week long Llaneras model of ischemic mitral regurgitation in sheep [16] and in comparison to chronic cardiac disease in humans [3]. This implies that in our five-week long animal study, the remodeling process of the annular and subvalvular apparatus might have still been in progress. Fourth, leaflet geometries were reconstructed from a discrete marker set. This implies that potential leaflet wrinkles and folds between two markers are invisible to the analysis. Characterizing growth through in plane markers alone also limits our study to membrane growth and does not allow us to quantify thickness changes, which typically accompany leaflet area changes [5]. Last, we would like to point out that it would have been valuable to collect data on the degree of regurgitation and correlate it with the degree of leaflet growth. Unfortunately, these data were not collected and these issues remain to be addressed in future studies.

5. CONCLUSION

In this study we have, for the first time, quantified regional and directional growth in the anterior mitral leaflet in the beating heart under acute and chronic ischemic conditions. On the annular level, chronic ischemia induced a significant chronic increase in mitral annular area, commissure-commissure distance, and septal-lateral distance. On the leaflet level, these events induced area growth, associated with chronic circumferential and radial leaflet elongations. Our observations suggest that mitral leaflets have the capacity to actively adapt to ventricular remodeling, and that mitral regurgitation may reflect a lack of this active adaptation. Further research will be necessary to elucidate the mechanotransduction pathways of mitral leaflet growth and to potentially correlate the leaflet's inability to grow to a genetic origin.

Acknowledgments

We thank Paul Chang for technical assistance and Maggie Brophy for careful marker image digitization, and George T. Daughters III for computation of 4D data from biplane 2D marker coordinates. This work was supported in part by the National Institutes of Health grants R01 HL29589 and R01 HL67025 to D. Craig Miller, and by the National Science Foundation CAREER award CMMI-0952021 to Ellen Kuhl.

References

1. Bothe W, Kuhl E, Kvitting JPE, Rausch MK, Göktepe S, Swanson JC, Farahmandnia S, Ingels NB, Miller DC. Rigid, complete annuloplasty rings increase anterior mitral leaflet strains in the normal beating ovine heart. Circulation. 2011; 124:S81–S96. [PubMed: 21911823]
2. Buganza Tepole AB, Ploch CJ, Wong J, Gosain AK, Kuhl E. Growing skin: A computational model for skin expansion in reconstructive surgery. J Mech Phys Solids. 2011; 59:2177–2190. [PubMed: 22081726]
3. Chaput M, Handschumacher MD, Tournoux F, Hua L, Guerrero JL, Vlahakes GJ, Levine RA. Mitral leaflet adaptation to ventricular remodeling: Occurrence and adequacy in patients with functional mitral regurgitation. Circulation. 2008; 118:845–852. [PubMed: 18678770]

4. Chaput M, Handschumacher MD, Guerrero JL, Holmvang G, Dal-Bianco JP, Sullivan S, Vlahakes GJ, Hung J, Levine RA. Mitral leaflet adaptation to ventricular remodeling: Prospective changes in a model of ischemic mitral regurgitation. Circulation. 2009; 120:S99–S103. [PubMed: 19752393]
5. Dal-Bianco JP, Aikawa E, Bischoff J, Guerrero JL, Handschumacher MD, Sullivan S, Johnson B, Titus JS, Iwamoto Y, Wylie-Sears J, Levine RA, Carpentier A. Active adaptation of the tethered mitral valve: Insights into a compensatory mechanism for functional mitral regurgitation. Circulation. 2009; 120:334–342. [PubMed: 19597052]
6. De Filippo RE, Atala A. Stretch and growth: the molecular and physiologic influences of tissue expansion. Plast Reconstr Surg. 2002; 109:2450–2462. [PubMed: 12045576]
7. Gillam LD. Is it time to update the definition of functional mitral regurgitation? Structural changes in the mitral leaflets with left ventricular dysfunction. Circulation. 2008; 118:797–799. [PubMed: 18711022]
8. Göktepe S, Bothe W, Kvitting JPE, Swanson JC, Ingels NB, Miller DC, Kuhl E. Anterior mitral leaflet curvature in the beating ovine heart: A case study using videofluoroscopic markers and subdivision surfaces. Biomech Model Mechanobio. 2010; 9:281–293.
9. Göktepe S, Abilez OJ, Parker KK, Kuhl E. A multiscale model for eccentric and concentric cardiac growth through sarcomerogenesis. J Theor Bio. 2010; 265:433–442. [PubMed: 20447409]
10. Göktepe S, Abilez OJ, Kuhl E. A generic approach towards finite growth with examples of athlete's heart, cardiac dilation, and cardiac wall thickening. J Mech Phys Solids. 2010; 58:1661–1680.
11. Grande-Allen KJ, Borowski AG, Troughton RW, Houghtaling PL, Di-Paola NR, Moravec CS, Vesely I, Griffin BP. Apparently normal mitral valves in patients with heart failure demonstrate biochemical and structural derangements. J Am Coll Cardiol. 2005; 45:54–61. [PubMed: 15629373]
12. Hueb AC, Jatene FB, Moreira LFP, Pomerantzeff PM, Kallas E, de Oliveira SA. Ventricular remodeling and mitral valve modifications in dilated cardiomyopathy: New insights from anatomic study. J Thorac Cardiovasc Surg. 2002; 124:1216–1224. [PubMed: 12447190]
13. Jaalouk DE, Lammerding J. Mechanotransduction gone awry. Nat Rev Mol Cell Biol. 2009; 10:63–73. [PubMed: 19197333]
14. Komeda M, Glasson JR, Bolger AF, Daughters GT, Ingels NB, Miller DC. Papillary muscle-left ventricular wall complex. J Thorac Cardiovasc Surg. 1997; 113:292–300. [PubMed: 9040623]
15. Kvitting JP, Bothe W, Gktepe S, Rausch MK, Swanson JC, Kuhl E, Ingels NB, Miller DC. Anterior mitral leaflet curvature during the cardiac cycle in the normal ovine heart. Circulation. 2010; 122:1683–1689. [PubMed: 20937973]
16. Llaneras MR, Nance ML, Streicher JT, Linden PL, Downing SW, Lima JA, Deac R, Edmunds LH. Pathogenesis of ischemic mitral insufficiency. J Thorac Cardiovasc Surg. 1993; 105:439–442. [PubMed: 8445923]
17. Niczyporuk M, Miller D. Automatic tracking and digitization of multiple radiopaque myocardial markers. Comp Biomed Res. 1991; 24:129–142.
18. Otsuji Y, Handschumacher MD, Schwammenthal E, Jiang L, Song JK, Guerrero JL, Vlahakes GJ, Levine RA. Insights from three-dimensional echocardiography into the mechanism of functional mitral regurgitation: direct in vivo demonstration of altered leaflet tethering geometry. Circulation. 1997; 96:1999–2008. [PubMed: 9323092]
19. Prot V, Skallerud B, Holzapfel GA. Transversely isotropic membrane shells with application to mitral valve mechanics. Constitutive modelling and finite element implementation. Int J Num Meth Eng. 2007; 71:987–1008.
20. Prot V, Skallerud B, Sommer G, Holzapfel GA. On modelling and analysis of healthy and pathological human mitral valves: Two case studies. J Mech Behav Biomed Mater. 2010; 3:167–177. [PubMed: 20129416]
21. Rausch MK, Bothe W, Kvitting JPE, Göktepe S, Miller DC, Kuhl E. In vivo dynamic strains of the ovine anterior mitral valve leaflet. J Biomech. 2011; 44:1149–1157. [PubMed: 21306716]
22. Rausch MK, Bothe W, Kvitting J-PE, Swanson JC, Ingels NB, Miller DC, Kuhl E. Characterization of mitral valve annular dynamics in the beating heart. Ann Biomed Eng. 2011; 39:1690–1702. [PubMed: 21336803]

23. Rausch MK, Dam A, Göktepe S, Abilez OJ, Kuhl E. Computational modeling of growth: Systemic and pulmonary hypertension in the heart. Biomech Mod Mechanobio. 2011; 10:799–811.
24. Rausch MK, Bothe W, Kvitting J-PE, Swanson JC, Miller DC, Kuhl E. Mitral valve annuloplasty: A quantitative clinical and mechanical comparison of different annuloplasty devices. Ann Biomed Eng. 2012; 40:750–761. [PubMed: 22037916]
25. Smuts AN, Blaine DC, Scheffer C, Weich H, Doubell AF, Dellimore KH. Application of finite element analysis to the design of tissue leaflets for a percutaneous aortic valve. J Mech Behav Biomed Mater. 2011; 4:85–98. [PubMed: 21094482]
26. Timek TA, Lai DT, Tibayan F, Daughters GT, Liang D, Dagum P, Lo S, Miller DC, Ingels NB. Atrial contraction and mitral annular dynamics during acute left atrial and ventricular ischemia in sheep. Am J Physiol Heart Circ Physiol. 2002; 283:H1929–H1935. [PubMed: 12384471]
27. Timek TA, Lai DT, Dagum P, Liang D, Daughters GT, Ingels NB, Miller DC. Mitral leaflet remodeling in dilated cardiomyopathy. Circulation. 2006; 114:I518–I523. [PubMed: 16820630]
28. Tsamis A, Bothe W, Kvitting JP, Swanson JC, Miller DC, Kuhl E. Active contraction of cardiac muscle: In vivo characterization of mechanical activation sequences in the beating heart. J Mech Behavior Biomed Mat. 2011; 4:1167–1176.
29. Tsamis A, Cheng A, Nguyen TC, Langer F, Miller DC, Kuhl E. Kinematics of cardiac growth: In vivo characterization of growth tensors and strains. J Mech Behavior Biomed Mat. 2012; 8:165–177.
30. Yiu SF, Enriquez-Sarano M, Tribouilloy C, Seward JB, Tajik AJ. Determinants of the degree of functional mitral regurgitation in patients with systolic left ventricular dysfunction: A quantitative clinical study. Circulation. 2000; 102:1400–1406. [PubMed: 10993859]
31. Zöllner AM, Buganza Tepole A, Kuhl E. On the biomechanics and mechanobiology of growing skin. J Theor Bio. 2012; 297:166–175. [PubMed: 22227432]

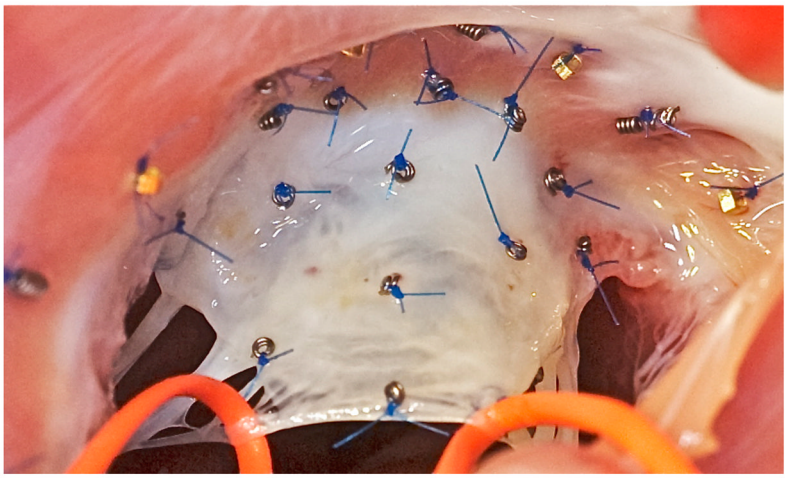

Figure 1.
Intraoperative photograph of the mitral annulus with the anterior mitral leaflet. Biplane videofluoroscopic imaging allows a precise spatial and temporal reconstruction of mitral valve dynamics both acutely and chronically.

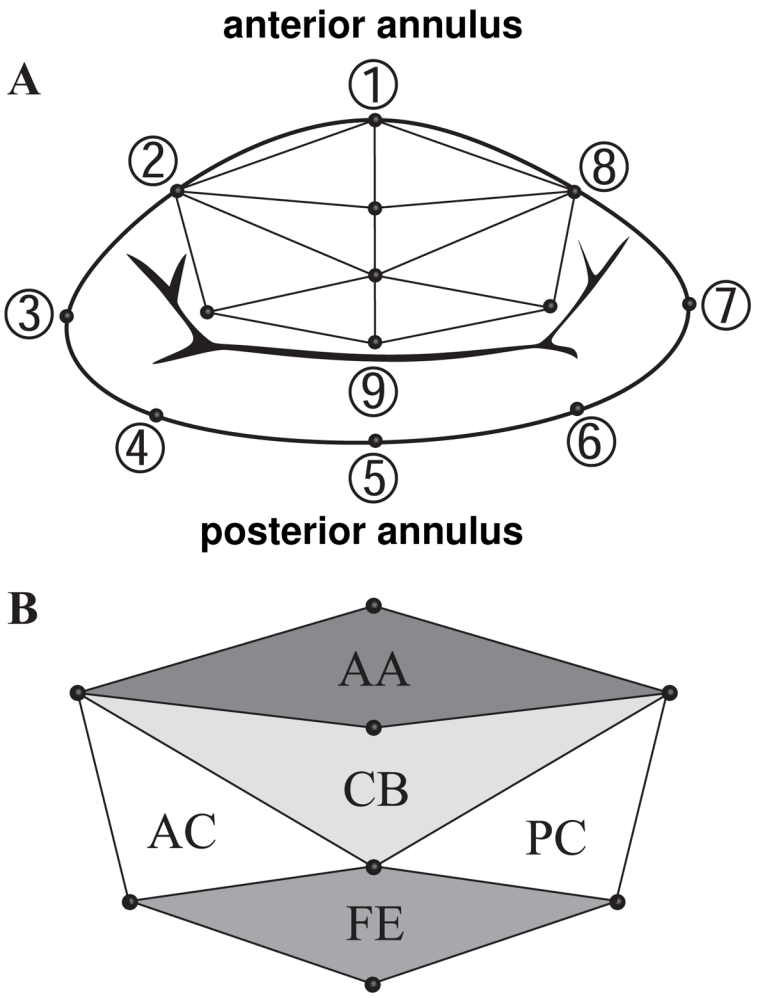

Figure 2.
Mitral annulus with anterior mitral leaflet. A) Marker locations and triangular mesh for regional strain analysis. B) Leaflet regions: Free Edge (FE), Central Belly (CB), Anterior Annulus (AA), Posterior Commissure (PC), and Anterior Commissure (AC).

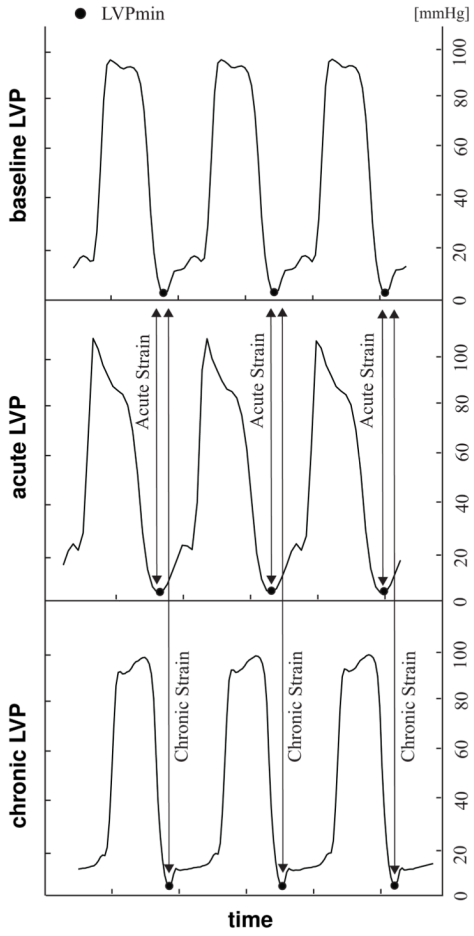

Figure 3.
Left ventricular pressure curves under baseline, acute, and chronic conditions. Acute strains are calculated for three consecutive cardiac cycles at minimum Left Ventricular Pressure (LVPmin) between baseline and acute conditions. Chronic strains are calculated for three consecutive cardiac cycles at LVPmin between baseline and chronic conditions.

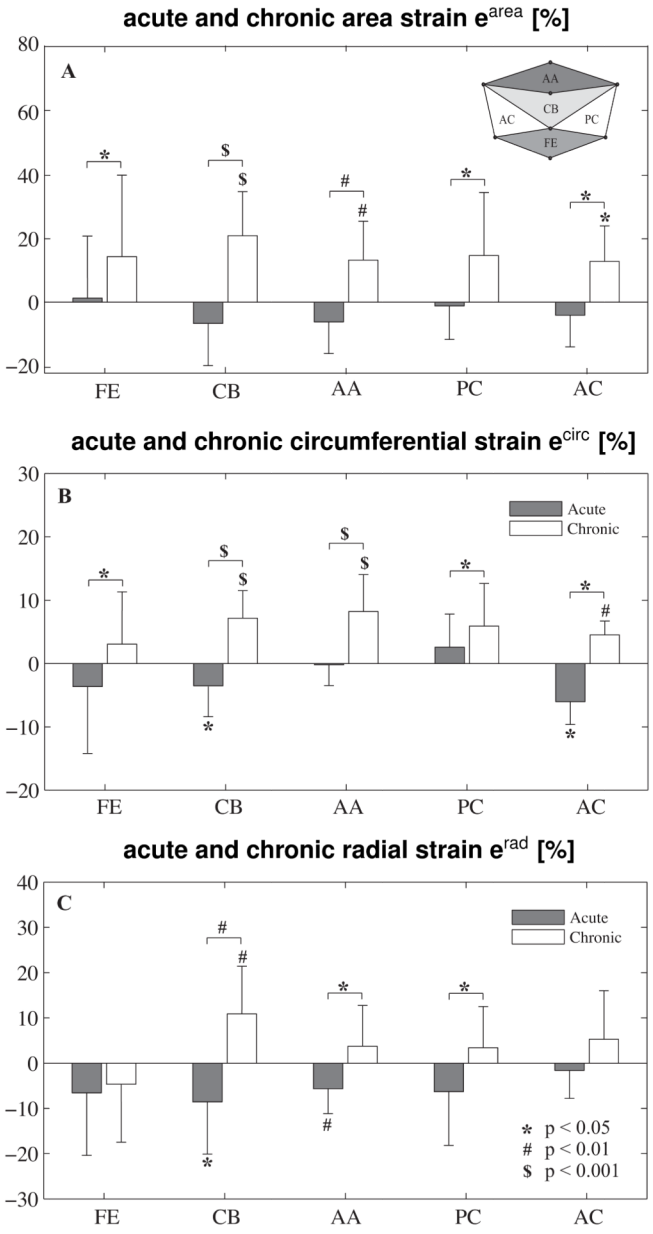

Figure 4.

Acute and chronic area, circumferential, and radial strains in different leaflet regions: Free Edge (FE), Central Belly (CB), Anterior Annulus (AA), Posterior Commissure (PC), and Anterior Commissure (AC). T-tests compare regional strains versus zero and acute and chronic strains. Anova compares strains between different regions.

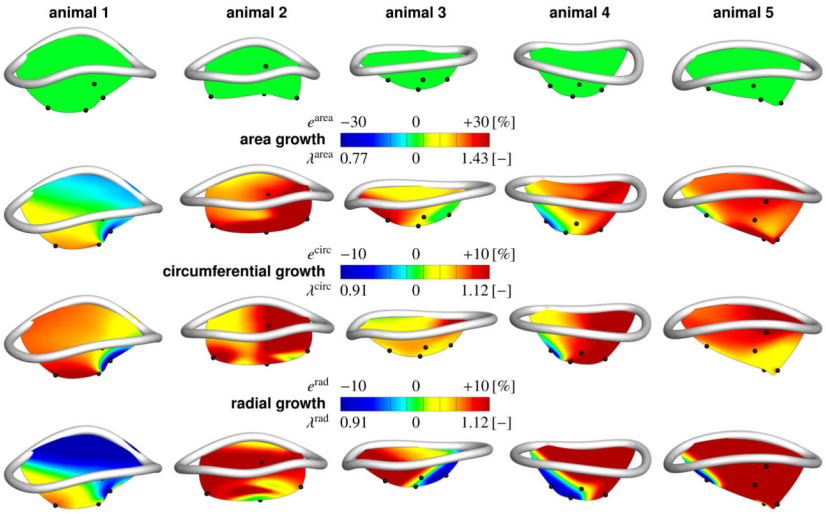

Figure 5.

Mitral annulus with anterior mitral leaflet. Normal annulus with leaflet at baseline conditions, first row. Chronic area strains e^{area} and stretches λ^{area}, second row. Chronic circumferential strains e^{circ} and stretches λ^{circ}, third row. Chronic radial strains e^{rad} and stretches λ^{rad}, fourth row. Strains and stretches are calculated between baseline and chronic conditions at minimum left ventricular pressure. Blue regions chronically decreased their area, and their circumferential and radial dimensions. Red regions chronically increased their area, and their circumferential and radial dimensions.

Table 1

Hemodynamics. Heart Rate (HR), dP/dt, maximum Left Ventricular Pressure (LVPmax), Left Ventricular End-Diastolic Pressure (LVEDP), Left Ventricular End-Systolic Pressure (LVESP), End-Diastolic Volume (EDV), and End-Systolic Volume (ESV). Reported are mean ± 1 standard deviation. Repeated-measure Anova was used to compare baseline, acute, and chronic hemodynamics.

	baseline mean ± 1 sd	acute mean ± 1 sd	chronic mean ± 1 sd	p
HR [1/min]	106.5 ± 9.0	126.0 ± 24.6	81.0 ± 6.3	0.027
dP/dt [mmHg/s]	1188.2 ± 369.1	1879.6 ± 848.2	862.3 ± 313.0	0.012
LVPmax [mmHg]	99.6 ± 10.9	97.0 ± 11.7	90.1 ± 11.5	0.528
LVEDP [mmHg]	19.6 ± 6.5	23.4 ± 10.6	17.2 ± 10.0	0.118
LVESP [mmHg]	86.7 ± 14.7	75.2 ± 5.6	78.4 ± 8.9	0.272
EDV [cc]	217.3 ± 122.2	220.6 ± 119.0	262.4 ± 97.7	0.340
ESV [cc]	155.5 ± 102.8	155.9 ± 118.8	179.0 ± 82.4	0.395

Table 2

Acute and chronic changes in cardiac geometry. Percent increases in annular dimensions and ventricular dimensions, and in Anterior Papillary Muscle (APM) displacements and Posterior Papillary Muscle (PPM) displacements, acutely and chronically in comparison to baseline conditions. Each first line compares changes at End Diastole (ED), each second line compares changes at End Systole (ES). Reported are mean ± 1 standard deviation (SD). Student t-tests were performed to test whether acute and chronic changes are larger than zero, whether chronic changes are larger than acute changes, and whether papillary muscle displacements are different from zero, acutely and chronically. Student t-test was employed to test whether papillary muscle displacements were different chronically from acutely.

annular changes						
		acute		**chronic**		
		mean ± 1 sd	**p > 0**	**mean ± 1 sd**	**p > 0**	**p >acute**
mitral annular	ED	− 5.05 ± 12.12	0.800	+32.50 ± 19.66	0.010	0.002
area [%]	ES	+ 2.65 ± 12.30	0.328	+18.34 ± 12.17	0.014	0.020
commissural	ED	− 4.36 ± 5.43	0.963	+14.11 ± 7.48	0.007	<0.001
distance [%]	ES	+ 2.02 ± 5.46	0.227	+ 9.52 ± 5.53	0.009	0.002
septal-lateral	ED	− 3.72 ± 5.63	0.893	+10.84 ± 6.48	0.010	0.006
distance [%]	ES	+ 0.76 ± 4.54	0.364	+ 5.57 ± 7.88	0.095	0.098
saddle	ED	−39.53 ± 127.78	0.736	−12.79 ± 33.58	0.221	0.182
height [%]	ES	−39.61 ± 16.02	0.003	−32.38 ± 38.48	0.067	0.691
anterior	ED	− 4.63 ± 5.56	0.315	+15.32 ± 5.15	0.003	0.007
perim. [%]	ES	+ 2.11 ± 6.01	0.534	+ 6.93 ± 5.85	0.008	0.008
posterior	ED	− 0.91 ± 6.50	0.882	+14.22 ± 7.04	0.007	0.001
perim. [%]	ES	+ 0.19 ± 0.29	0.382	+ 9.93 ± 7.06	0.011	0.014
ventricular changes						
		acute		**chronic**		
		mean ± 1 sd	p > 0	mean ± 1 sd	p > 0	p >acute
ventricular	ED	− 0.67 ± 3.83	0.641	+17.15 ± 4.56	<0.001	0.002
dilation [%]	ES	− 1.92 ± 2.29	0.933	+15.48 ± 5.81	0.002	0.001

annular changes						
	acute			chronic		
	mean ± 1 sd	p > 0		mean ± 1 sd	p > 0	p > acute
papillary muscle changes						
	acute			chronic		
	mean ± 1 sd		p ≠ 0	mean ± 1 sd	p ≠ 0	p ≠ acute
apical PPM	ED	− 0.27 ± 0.70	0.443	− 1.45 ± 4.65	0.523	0.570
displ. [mm]	ES	− 1.20 ± 1.42	0.132	− 0.88 ± 4.93	0.710	0.886
lateral PPM	ED	+ 0.48 ± 0.96	0.325	+ 0.08 ± 4.34	0.969	0.855
displ. [mm]	ES	+ 2.82 ± 1.71	0.021	+ 4.21 ± 3.76	0.067	0.459
posterior PPM	ED	+ 4.36 ± 8.36	0.308	+13.49 ± 12.31	0.070	0.012
displ. [mm]	ES	+ 2.06 ± 6.14	0.494	+11.89 ± 11.30	0.078	0.016
apical APM	ED	+ 0.00 ± 0.75	0.979	− 3.29 ± 1.37	0.006	0.013
displ. [mm]	ES	+ 0.82 ± 0.41	0.011	− 0.76 ± 1.37	0.284	0.070
lateral APM	ED	+ 0.03 ± 0.93	0.945	+ 0.70 ± 1.10	0.227	0.461
displ. [mm]	ES	+ 1.07 ± 0.68	0.024	+ 2.14 ± 2.49	0.126	0.370
posterior APM	ED	+ 0.11 ± 1.35	0.862	− 0.49 ± 2.13	0.623	0.566
displ. [mm]	ES	− 1.48 ± 0.91	0.022	− 1.76 ± 3.22	0.288	0.814